# Plasma Waves Near Saturn: Initial Results from Voyager 1

Abstract. *The Voyager 1 plasma wave instrument detected many familiar types of plasma waves during the encounter with Saturn, including ion-acoustic waves and electron plasma oscillations upstream of the bow shock, an intense burst of electrostatic noise at the shock, and chorus, hiss, electrostatic electron cyclotron waves, and upper hybrid resonance emissions in the inner magnetosphere. A clocklike Saturn rotational control of low-frequency radio emissions was observed, and evidence was obtained of possible control by the moon Dione. Strong plasma wave emissions were detected at the Titan encounter indicating the presence of a turbulent sheath extending around Titan, and upper hybrid resonance measurements of the electron density show the existence of a dense plume of plasma being carried downstream of Titan by the interaction with the rapidly rotating magnetosphere of Saturn.*

The Voyager 1 encounter with Saturn in November 1980 has now provided the first opportunity to investigate plasma wave interactions in the magnetosphere of Saturn. We now present an overview of the principal results from the Voyager 1 plasma wave instrument starting with the initial detection of Saturn and ending about 4 weeks after closest approach. A survey plot of the electric field intensities detected during the Saturn encounter is shown in Fig. 1, starting shortly before the inbound shock crossing and ending shortly after the outbound magnetopause crossing. Many intense waves were observed in the vicinity of Saturn. To provide a framework for presenting the observations, the results are discussed more or less according to the sequence in which the data were obtained. (The Saturn radio emissions are discussed last.) The Voyager plasma wave instrument has been described previously by Scarf and Gurnett (*1*).

*Upstream waves, shock, and magnetopause.* During the approach to Saturn, the solar wind upstream of Saturn was remarkably quiet. Occasionally, when the proper magnetic connection was available to the bow shock, brief bursts of ion-acoustic waves were detected with characteristics similar to those detected upstream of Jupiter's bow shock (*2*). Saturn's bow shock was encountered at 2327 spacecraft event time (SCET) on 11 November at a radial distance of 26.2 Saturn radii ($R_S$) (Fig. 1). A brief burst of electron plasma oscillations occurred ahead of the shock which was followed by an intense burst of broadband electric field noise at the shock with characteristics similar to the bow shock at Jupiter (*2*). Downstream of the shock, the electric field intensities in the magnetosheath were low. Five magnetopause crossings were observed on the inbound pass with the first and last occurring at 0154 and 0248 on 12 November (Fig. 1). At each magnetopause crossing, a brief narrowband burst of electric field noise occurred in the 5.62-kHz channel, probably as a result of either electron plasma oscillations or upper hybrid resonance (UHR) emissions. In the outer regions of the magnetosphere, the electric field intensities again returned to low levels. No evidence was found for trapped continuum radiation comparable to that observed in the magnetospheres of Earth or Jupiter (*2*).

*Titan encounter.* One of the main targeting objectives of the Voyager 1 encounter with Saturn was a close flyby of the moon Titan, which was inside the magnetosphere at the time of the encounter. The close flyby provided a good opportunity to study the interaction of Titan with the rapidly rotating magnetospheric plasma of Saturn, which flows by at a nominal velocity of about 200 km/sec. Several major effects were observed in the plasma wave data near Titan. Two regions of intense low-frequency electric-field turbulence were detected in the vicinity of Titan (Fig. 2). The spectrum and qualitative characteristics of this turbulence resemble those of the electrostatic turbulence in the magnetosheath and ionosheath of Earth and Venus (*3*). These similarities suggest the existence of a turbulent sheathlike region extending around Titan (Fig. 2). This turbulence is believed to consist of ion-acoustic waves driven by currents and nonequilibrium plasma distributions in the sheath. A pronounced asymmetry is evident in the thickness of the sheath and the spectrum of the noise on the inbound and outbound passes. Corresponding asymmetries with almost identical boundaries are also evident in the magnetic field signature reported by the Voyager magnetometer team (*4*). The initial intense burst of noise at 0532:30 suggests a shocklike interaction at the upstream boundary of the sheath. Although the flow is likely to be sub-Alfvénic, the interaction might be a slow-mode shock.

At frequencies above 5 kHz, a series of narrowband emissions sweeps through adjacent frequency channels (Fig. 2). On the basis of the similarity to narrowband upper hybrid emissions observed in the magnetosphere of Earth (*5*), we believe these emissions to be

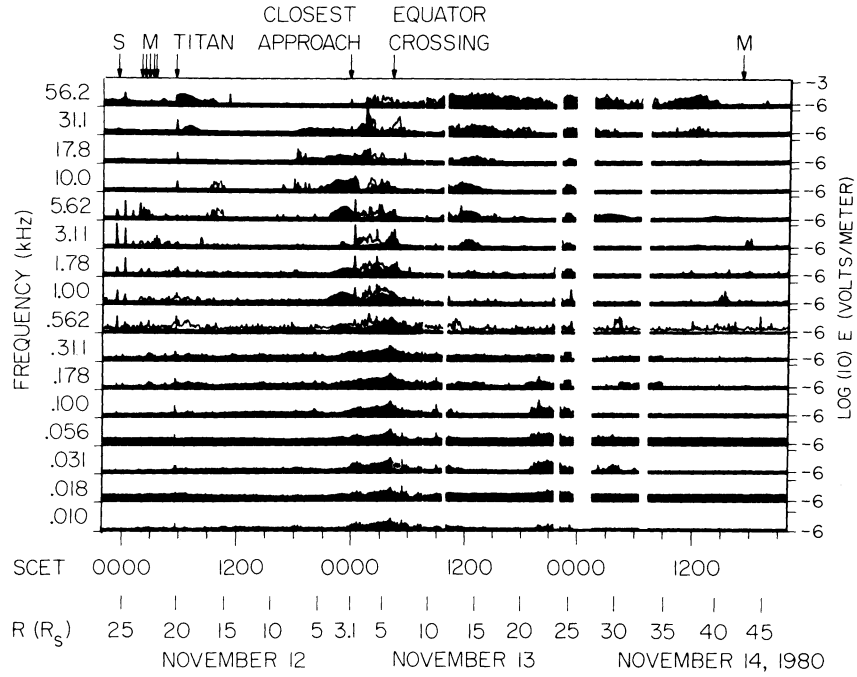


Fig. 1. An overview of the electric field intensities detected for a 3-day period starting shortly before the inbound shock crossings (*S*) and ending shortly after the outbound magnetopause crossing (*M*). Strong plasma wave intensities were observed at the Titan flyby (shown expanded in Fig. 2) and through the inner region of the magnetosphere near closest approach. The intense signals in the 3.11- to 56.2-kHz channels about 1200 on 13 November are radio emissions from Saturn.


0036-8075/81/0410-0235$01.00/0 

at the local UHR frequency $f_{UHR} = \sqrt{f_p^2 + f_g^2}$, where $f_p$ and $f_g$ are the electron plasma frequency and gyrofrequency. Since $f_g \ll f_p$, the UHR emission frequency provides a direct determination of the local electron density, $N = (f_p/9000)^2$ cm$^{-3}$. In Fig. 2, the smooth dashed line through the circled UHR emissions gives our initial determination of the electron density profile (read from the scale on the left). These measurements show that the peak electron density in the wake of Titan, ~ 40 cm$^{-3}$, is several orders of magnitude larger than the electron density in the surrounding magnetosphere, ~ 0.01 to 0.1 cm$^{-3}$. The high densities in the wake, the steep density gradients, and the alignment of the density maximums with the sheath boundaries suggest that the spacecraft has passed through a dense plume of plasma that is being swept away from Titan by the magnetospheric interaction. The density profile of the wake disturbance appears to be shifted about 10° to 20° toward Saturn with respect to the plasma flow expected for rigid corotation.

Coincident with the exit from the region of enhanced density, an abrupt onset of radio emissions can be seen at about 0542:40 in the 56.2-kHz channel of Fig. 2. The intensity of this radio emission gradually decreases to the instrument noise level over a 2-hour period after the Titan encounter (Fig. 1). Two interpretations of this radio emission have been proposed. The abrupt onset of the radiation at Titan and the gradual decrease in intensity with increasing radial distance from Titan seem to indicate that Titan is the source. The source would then have to be on the Saturn-facing side of Titan (Fig. 2). The occurrence of intense UHR emissions on the same side of Titan suggests that the generation mechanism may be the same as continuum radiation at Earth, which is probably generated by UHR emissions at the plasmapause (*5*). Since Saturn also emits radio noise in the same frequency range, Saturn must also be considered as a possible source. If Saturn is the source, the abrupt onset at Titan could be a propagation cutoff caused by the high electron density near Titan. Although we have no results that can definitely eliminate Saturn as the source, examination of temporal fluctuations shows that the radiation associated with Titan has characteristics different from the typical Saturn radio emissions.

*Magnetosphere*. Within the magnetosphere, the greatest plasma wave activity occurs inside about 10 $R_S$. A detailed plot of the electric field intensities in the region near closest approach is shown in Fig. 3. To interpret the plasma wave intensities, we must know $f_g$ and $f_p$. The $f_g$ profile ($f_g = 28B$ Hz, where $B$ is the magnetic field in gammas) (solid line in Fig. 3) can be determined from the magnetic field measurements (*4*). The $f_p$ profile is more difficult to determine and must be obtained by a combination of interpretation and comparison with direct measurements (*6*). For example, the brief bursts of electron plasma oscillations from about 1800 to 2000 on 12 November show $f_p$ between 10 and 17.8 kHz. Past 2000, a band of radio emission can be seen in the high-frequency channels with a well-defined low-frequency cutoff. The cutoff first decreases, reaches a minimum of about 3 kHz at 2300 on 12 November, and then increases to about 31.1 kHz at 0130 on 13

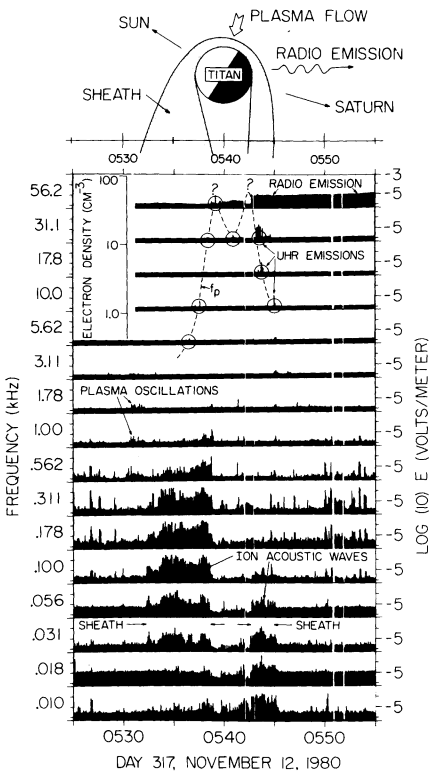


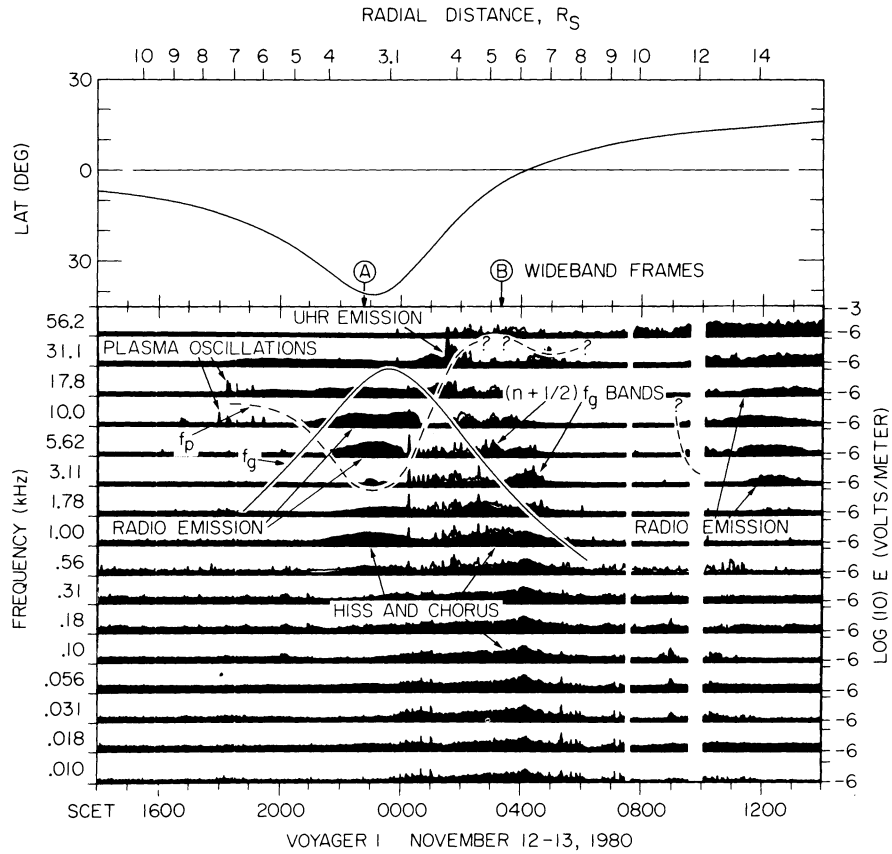


Fig. 2 (left). Equatorial plane projection of the spacecraft trajectory near Titan (top) and the corresponding electric field intensities (bottom). The intense low-frequency noise suggests the existence of a highly turbulent sheath region extending around Titan. The electron density profile (dashed line) determined from upper hybrid resonance (*UHR*) emissions (circles) shows that a dense plume of plasma extends into the downstream wake, apparently being carried away by the magnetospheric interaction. The question marks indicate uncertainties about the peak densities because of the absence of measurements above 56.2 kHz. Fig. 3 (right). The plasma wave electric field intensities in the region near closest approach. The dashed line gives the approximate electron plasma frequency ($f_p$) profile derived from a combination of electron plasma oscillations, radio emission propagation cutoffs, and UHR emissions. Question marks indicate regions of uncertainty in the profile. The electron gyrofrequency ($f_g$) profile was obtained from the magnetometer. Arrows marked *A* and *B* refer to spectrograms in Fig. 5.

November, when an intense UHR emission occurs. This cutoff seems to be at $f_p$, which represents the low-frequency limit of the free-space electromagnetic mode. Although the cutoff provides only an upper limit for the local plasma frequency, comparisons with the electron densities from the plasma instrument (*6*) at a few isolated points show that the cutoff is close to the local $f_p$. The resulting $f_p$ contour is shown by the dashed line in Fig. 3. After about 0200 on 13 November it becomes difficult to determine the $f_p$ profile. The UHR emissions at about 0500 indicate that $f_p$ is near 31.1 kHz then; after 0900 $f_p$ again drops to 3 kHz or less, as shown by the high-frequency radio emissions extending down into the 3.11-kHz channel after this time.

The interpretation of these plasma frequency variations is illustrated in Fig. 4, which shows a meridian plane projection of the spacecraft trajectory. Two principal effects are noted, namely that $f_p$, and hence the electron density, is very low ($< 1$ cm$^{-3}$) from about 2030 on 12 November to 0100 on 13 November and again after 0900 on 13 November. Under the assumption that the plasma density distribution is symmetrical with respect to the rotational axis of Saturn, these variations represent penetrations into low-density regions north and south of a dense equatorially confined plasma torus. In the central region of the torus, the electron densities range from about 10 to 40 cm$^{-3}$, which are consistent with the Pioneer 11 measurements of Frank *et al.* (*7*). The north-south thickness of the torus is about 4 $R_S$.

Further identification of the plasma wave emissions in Fig. 3 is assisted by the 48-second frames of wideband waveform data obtained near closest approach (Fig. 5). Spectrogram A was obtained at 2251:46 on 12 November, shortly before closest approach, and spectrogram B was obtained at 0326:10 on 13 November, shortly before crossing the equatorial plane. Both spectrograms show a strong band of noise at frequencies below 2 kHz, in the frequency range appropriate for the whistler mode ($f \lesssim f_g$ and $f \lesssim f_p$). Spectrogram B shows that this noise consists of discrete tones and a relatively steady band of noise that resembles the whistler-mode chorus and hiss emissions observed in the terrestrial and Jovian magnetospheres (*8*). In spectrogram A, the chorus is completely absent and the emission appears to consist entirely of hiss. The survey plot in Fig. 3 shows that the whistler-mode emissions reached maximum intensity at about 0410 on 13 November, coincident with the equatorial plane crossing. Preliminary estimates indicate that the chorus and hiss emissions in this region are in resonance with electrons of relatively low energy, between 1 and 5 keV.

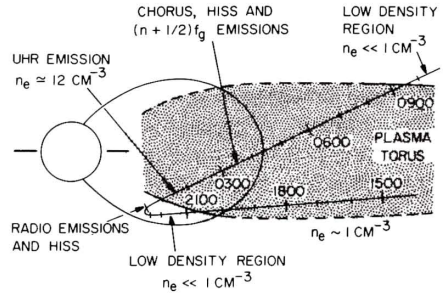


Fig. 4. A meridian plane plot of the spacecraft trajectory showing the regions of low electron density determined from the electron $f_p$ profile in Fig. 3. The highest electron densities were encountered inside a torus-like region with a north-south thickness of about 4 $R_S$.

Figure 5B shows another series of emissions slightly above $f_g$, $2f_g$, and $3f_g$. These emissions are electrostatic electron cyclotron waves of the type observed in both the terrestrial and Jovian magnetospheres (*9*). They tend to occur near half-integral harmonics of the electron cyclotron frequency and are identified in Fig. 3 as $(n + 1/2)f_g$ bands. Figure 5A shows a large number of puzzling bands. Several characteristic frequency spacings can be identified, including about 875 Hz, 1.45 kHz, and 3.90 kHz. None of these band spacings are related to the local $f_g$, which is 25.3 kHz. These emissions are believed to be propagating in the free-space electromagnetic mode since they can be detected at the same frequency over a wide range of radial distances. In considering the origin of these narrowband electromagnetic emissions, we suggest that they are probably generated by conversion from electrostatic $(n + 1/2)f_g$ emissions near the upper hybrid resonance, in a way similar to the generation of continuum radiation in the terrestrial magnetosphere (*10*). If the characteristic frequency spacings correspond to the electron gyrofrequency in the plasma torus, the emissions would originate from about 8.6, 7.3, and 5.2 $R_S$.

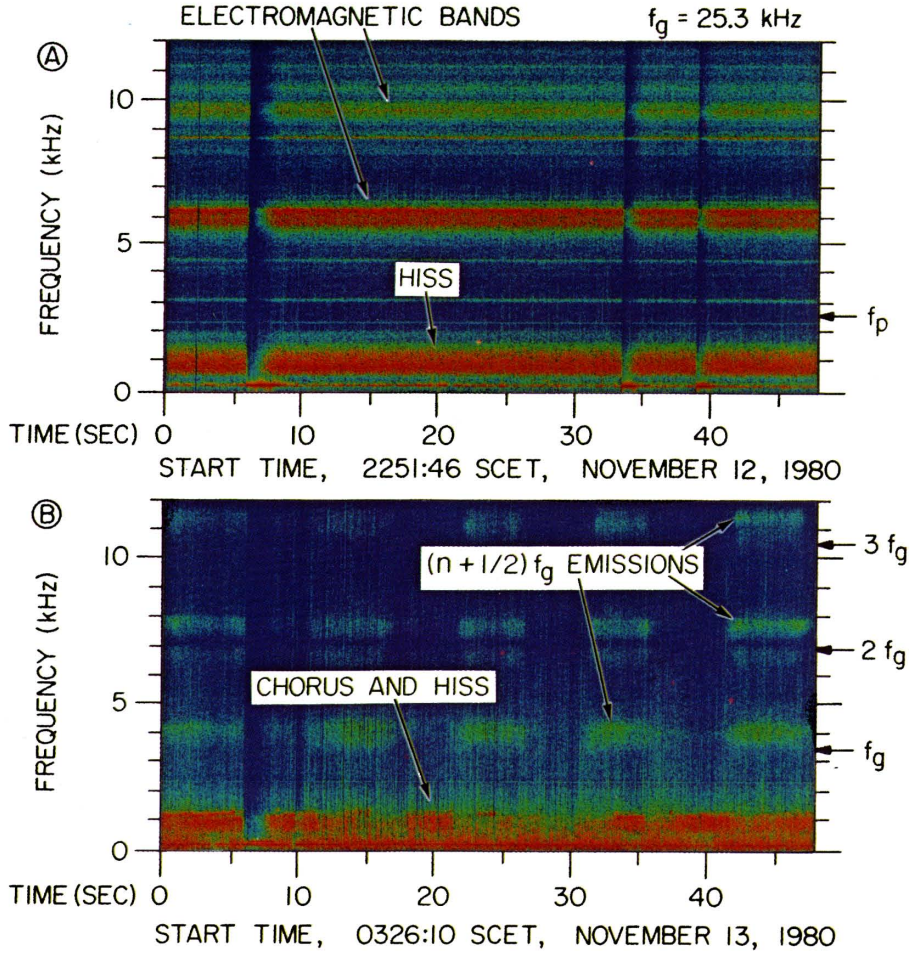


Fig. 5. Wideband spectrograms from points *A* and *B* in Fig. 3. A band of whistler-mode hiss and chorus is evident in both spectrograms at frequencies below about 2 kHz. In (B), the diffuse emissions slightly above the $f_g$ harmonics are electrostatic electron cyclotron waves. The intense bands at about 6 and 9.6 kHz in (A) are electromagnetic waves propagating in the left-hand ordinary mode at frequencies above the local electron $f_p$ (2.4 kHz), which was determined through the use of the electron density from the plasma instrument.

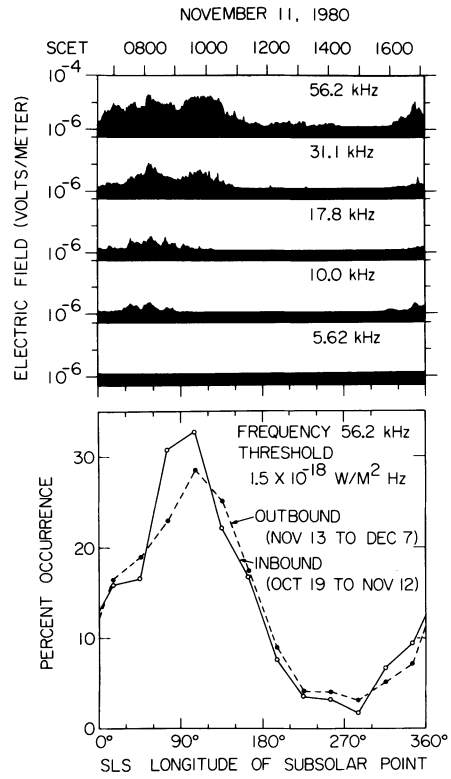


Fig. 6. The top panel shows a representative Saturn radio emission event. The time scale corresponds to one rotation of Saturn. The bottom panel shows the emission probability at 56.2 kHz as a function of the subsolar longitude, using the PRA Saturn longitude system (*SLS*).

These radial distances are close to the orbits of Rhea, Dione, and Tethys, which suggests that these moons may be involved in the generation of the radio emissions.

Near closest approach, we also carried out a search for lightning-generated whistlers. Many impulsive signals were detected near closest approach, some of which can be seen in Fig. 5B. However, none of these signals appear to have dispersion characteristics consistent with whistlers generated by lightning in Saturn's atmosphere. The origin of these impulsive signals is still being investigated. Other possibilities being considered include Doppler-shifted ion-acoustic waves, electrostatic discharges on the spacecraft, and spacecraft-generated interference.

During the outbound pass through the high-latitude region of the magnetosphere, the intensities again dropped to low levels. No indication was found for intense low-frequency continuum radiation of the type observed in the magnetotail of Jupiter (*2*). The main effect of interest in the high-latitude magnetotail is the intense low-frequency electric field noise evident in Fig. 1 from about 1930 to 2400 on 13 November. This noise resembles the broadband electrostatic noise observed along the auroral field lines in the terrestrial magnetosphere (*11*). This noise also occurs at *L*-values consistent with the observed location of the aurora at Saturn (*12*).

*Saturn radio emissions.* Several months before the Voyager 1 encounter with Saturn, the Planetary Radio Astronomy (PRA) team identified strong nonthermal radio emissions originating from Saturn's magnetosphere (*13*). These radio emissions are most intense in the kilometer wavelength range and are strongly controlled by the rotation of Saturn. The rotational period was determined to be 10 hours and 39.4 minutes. Because the peak in the emission spectrum occurs slightly above the frequency range of the plasma wave instrument, these radio emissions were not regularly detected in the plasma wave data until about 6 weeks before closest approach. Initially, the signals were detected only in the highest frequency channel. As the spacecraft approached Saturn, however, the intensities increased rapidly and it became possible to detect the radio emissions at much lower frequencies, sometimes as low as 3 kHz. Figure 6, for example, shows a typical radio event plotted over a time interval corresponding to one complete rotation. The time origin has been selected to correspond to the time when the sun is at 0° longitude in the Saturn Longitude System (SLS) (*13*). The emission is most intense in the highest, 56.2-kHz, channel and lasts for about one-half of a Saturn rotation with maximum intensity when the subsolar longitude is near 90°.

A basic question concerning the radio emission process is whether the rotational control is caused by a radiation pattern which rotates with the planet, like a rotating searchlight, or whether the modulation is a temporal effect, like a flashing light. These two models can be tested by comparing the phase of the rotational modulation on the inbound and outbound passes. If the modulation is caused by the searchlight effect, the phase should shift by an amount corresponding to the angle between the inbound and outbound trajectories projected into the equatorial plane, which is about 135°. The rotational modulation for the inbound and outbound passes is illustrated in the bottom panel of Fig. 6. The absence of a phase difference between the inbound and outbound passes implies that the control is a temporal or clocklike effect, in which the radiation is emitted simultaneously over a wide range of directions at a particular phase of Saturn's rotation. Because of the very small tilt of the magnetic dipole axis of Saturn with respect to the rotational axis (*4*, *14*), the origin of this pronounced rotational control is difficult to understand. We think it most likely, for example, that the modulation is caused by a high-order distortion of the magnetic field near the planet, but the mechanism

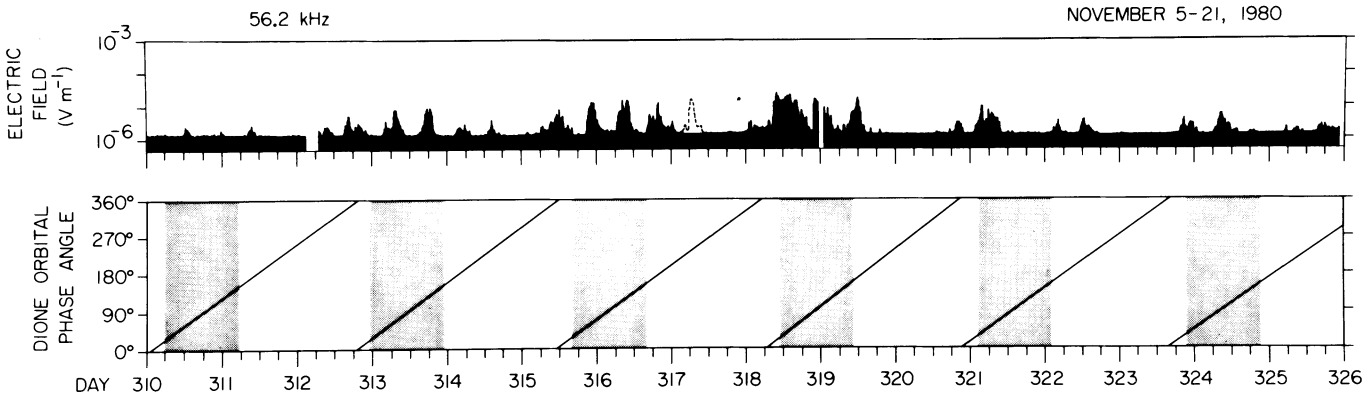


Fig. 7. A 16-day plot showing the long-term quasi-periodic modulation of the Saturn radio burst intensities. This modulation appears to be controlled by the orbital position of Dione, with the largest intensities occurring as Dione passes through the local morning region of the magnetosphere. The orbital phase angle is measured positive eastward from a plane containing the sun and the rotational axis of Saturn, with 0° at local midnight.

Fig. 8. The radio emission intensity at 56.2 kHz as a function of the subsolar SLS longitude and the Dione orbital phase angle.

by which this distortion could affect the radio emission is not clear.

Although Saturn's rotation has a major effect on the radio emission process, other factors are also involved since the intensity of the events varies substantially on time scales of days. Figure 7 shows a 16-day plot of the 56.2-kHz intensities centered on closest approach. In addition to the basic rotational control an overall modulation of the intensities can be seen with a period slightly less than 3 days. For instance, intense events are present on days 313, 316, 318 and 319, 321, and 324. Because of the well-known control of Jovian radio emissions by the moon Io, an obvious explanation of this periodicity is that one of the moons of Saturn is influencing its radio emissions. Dione is the only moon with a suitable period, 2.74 days. The orbital phase angle of Dione is shown in the bottom panel of Fig. 7. The correlation appears to be quite good. A further analysis using all of the available data shows the radio emission intensity at 56.2 kHz as a function of both the subsolar SLS longitude and the Dione orbital phase (Fig. 8). The significance of the combined control by these two parameters is best seen by comparing the relative intensities in the upper left and lower right quadrants. The largest radio emission intensities occur when the subsolar SLS longitude is near 90° and Dione is passing through the local morning region of the magnetosphere. The best correlation with Dione's position occurs during the few weeks around closest approach, when the intensities are largest.

The apparent control of the Saturnian radio emission intensities by Dione suggests that this moon may be involved in a strong magnetospheric interaction, possibly resembling the interaction of Io with the Jovian magnetosphere. Most likely this interaction would imply outgassing and production of plasma by Dione, similar to the situation at Io. Although there is no evidence of volcanic activity, the photographs of Dione show white wispy features indicating the loss of volatile material (*15*). Furthermore, the Pioneer 11 plasma measurements show a peak in the plasma density profile near Dione's orbit (*7*), suggesting that Dione is a source of plasma. If Dione is injecting plasma into the magnetosphere, numerous mechanisms could account for the dependence on orbital position, including magnetospheric

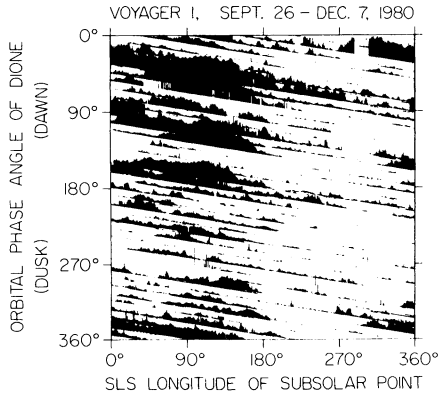


dawn-dusk asymmetries, propagation effects due to Dione-induced density variations in the plasma torus, and phase variations in the outgassing rate due to surface asymmetries on Dione.

D. A. GURNETT
W. S. KURTH
*Department of Physics and Astronomy, University of Iowa, Iowa City 52242*
F. L. SCARF
*Space Sciences Department, TRW Defense and Space Systems Group, Redondo Beach, California 90278*

### References and Notes

1. F. L. Scarf and D. A. Gurnett, *Space Sci. Rev.* **21**, 289 (1977).
2. ———, W. S. Kurth, *Science* **204**, 991 (1979); D. A. Gurnett, *et al.*, *ibid.* **206**, 987 (1979).
3. P. Rodriguez, *J. Geophys. Res.* **84**, 917 (1979); F. L. Scarf, W. W. L. Taylor, C. T. Russell, R. C. Elpic, *ibid.* **85**, 7599 (1980).
4. N. F. Ness, M. H. Acuña, R. P. Lepping, J. E. P. Connerney, K. W. Behannon, L. F. Burlaga, F. M. Neubauer, *Science* **212**, 211 (1981).
5. R. R. Shaw and D. A. Gurnett, *J. Geophys. Res.* **80**, 4259 (1975); W. S. Kurth, J. D. Craven, L. A. Frank, D. A. Gurnett, *ibid.* **84**, 4145 (1979); K. Rönnmark, H. Borg, P. J. Christiansen, M. P. Gough, D. Jones, *Space Sci. Rev.* **22**, 401 (1978).
6. H. S. Bridge *et al.*, *Science* **212**, 217 (1981).
7. L. A. Frank, B. G. Burek, K. L. Ackerson, J. H. Wolfe, J. D. Mihalov, *J. Geophys. Res.* **85**, 5695 (1980).
8. G. McK. Allcock, *Austr. J. Phys.* **10**, 286 (1957); C. T. Russell, R. E. Holtzer, E. J. Smith, *J. Geophys. Res.* **74**, 755 (1969); F. L. Scarf, D. A. Gurnett, W. S. Kurth, in (*2*); F. V. Coroniti, F. L. Scarf, C. F. Kennel, W. S. Kurth, D. A. Gurnett, *Geophys. Res. Lett.* **7**, 45 (1980).
9. C. F. Kennel, F. L. Scarf, R. W. Fredricks, J. H. McGehee, F. V. Coroniti, *J. Geophys. Res.* **75**, 6136 (1970); W. S. Kurth, D. D. Barbosa, D. A. Gurnett, F. L. Scarf, *Geophys. Res. Lett.* **7**, 57 (1980).
10. D. A. Gurnett and R. R. Shaw, *J. Geophys. Res.* **78**, 8136 (1973); D. A. Gurnett, *ibid.* **80**, 2751 (1975); W. S. Kurth, D. A. Gurnett, R. R. Anderson, *ibid.*, in press.
11. D. A. Gurnett and L. A. Frank, *ibid.* **82**, 1031 (1977); ———, R. P. Lepping, *ibid.* **81**, 6059 (1976).
12. A. L. Broadfoot *et al.*, *Science* **212**, 206 (1981).
13. M. L. Kaiser, M. D. Desch, J. W. Warwick, J. B. Pearce, *ibid.* **209**, 1238 (1980); M. D. Desch and M. L. Kaiser, *Geophys. Res. Lett.*, in press.
14. E. J. Smith *et al.*, *Science* **207**, 407 (1980); M. H. Acuña and N. F. Ness, *ibid.*, p. 444.
15. B. A. Smith *et al.*, *Science*, **212**, 163 (1981).
16. We thank the entire Voyager team at NASA Headquarters and the Jet Propulsion Laboratory (JPL) for their support. We are especially grateful to R. Poynter for his invaluable assistance and support. We also thank E. Miner and J. Diner for their efforts to arrange the wideband coverage; J. Anderson, P. Jepsen, and G. Garneau for their assistance with the wideband data processing; C. Stembridge for his help in solving numerous problems; H. Bridge, J. Belcher, J. Scudder, and N. Ness for providing data in advance of publication and for their helpful discussions; and R. Anderson, R. West, L. Granroth, and R. Brechwald for carrying out the data reduction. The research at the University of Iowa was supported by NASA through contract 954013 with JPL, through grants NGL-16-001-002 and NGL-16-001-043 from NASA Headquarters, and by the Office of Naval Research. The research at TRW was supported by NASA through contract 954012 with JPL.

9 February 1981